The Cellular Basis of a Corollary Discharge

James F. A. Poulet and Berthold Hedwig

Science **311**, 518 (2006);
DOI: 10.1126/science.1120847

Science (print ISSN 0036-8075; online ISSN 1095-9203) is published weekly, except the last week in December, by the American Association for the Advancement of Science, 1200 New York Avenue NW, Washington, DC 20005.

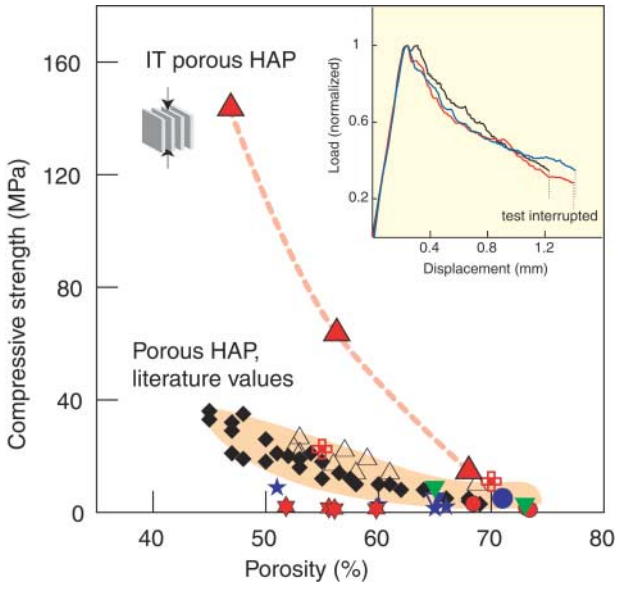

Fig. 4. Compressive strength of porous HAP scaffolds. Results from literature [blue stars (*22*), red stars (*23*), inverted green triangles (*24*), black triangle (*25*), blue circle (*26*), inverted blue triangle (*27*), diamonds (*28*), cross (*29*), and red circles (*30*)] versus IT porous HAP scaffolds. The typical pore sizes of conventional porous HAP scaffolds are on the order of 100 to 800 μm in order to allow bone ingrowth. In the IT materials exhibiting the greatest strength, the pores are typically ~20 by ~200 μm wide and several millimeters long; previous studies have indicated that these dimensions are adequate for bone tissue engineering (*20*). For the IT porous materials, compression is applied in the direction parallel to the ceramic layers. The presence of inorganic bridges between the ceramic layers (a feature that parallels the microstructure of nacre) prevents Euler buckling of the ceramic layers and contributes to the high strength. **(Inset)** Typical compression load-displacement curves for materials with 56% porosity (three different samples shown here). The samples fail gradually, and, because of the large degree of control of hierarchical architecture, the mechanical behavior is very consistent from one sample to another.

suspensions, we processed IT highly porous lamellar scaffolds that are four times stronger in compression than conventional porous HAP (Fig. 4). These IT scaffolds exhibit well-defined pore connectivity along with directional and completely open porosity of an adequate size to allow bone ingrowth (*20*). Hence, most of the current shortcomings (low strength, random organization, multiple pore size, and uncontrolled pore connectivity) that plague bone substitutes are eliminated by this innovative approach.

Current ceramic and metallic implant materials have serious shortcomings because of the mismatch of physical properties with those of bone. In bone, intrinsically weak materials, such as calcium phosphates and collagen, are combined into composites exhibiting intermediate modulus (10 to 20 GPa), fairly high strength (30 to 200 MPa), and high work of fracture (100 to 1000 J/m^2) (*21*). The unique properties of bone arise from the controlled integration of the organic (collagen) and inorganic (apatite) components (*5*) with a sophisticated architecture from the nano- to mesolevels. Our approach to the problem is to infiltrate the IT porous HAP scaffolds with a second organic phase with tailored biodegradability. Because the biodegradation rates of the scaffold and the infiltrated compound can be designed to be different, porosity can be created in situ to allow bone ingrowth. By using this approach, we have been able to fabricate HAP-based composites with stiffness (10 GPa), strength (150 MPa), and work of fracture (220 J/m^2) that match that of compact bone for an equivalent mineral/organic content (around 60/40 vol %).

References and Notes

1. G. Mayer, *Science* **310**, 1144 (2005).
2. C. Sanchez, H. Arribart, M. M. G. Guille, *Nat. Mater.* **4**, 277 (2005).
3. L. Addadi, S. Weiner, *Nature* **389**, 912 (1997).
4. B. L. Smith *et al.*, *Nature* **399**, 761 (1999).
5. G. E. Fantner *et al.*, *Nat. Mater.* **4**, 612 (2005).
6. Z. Y. Tang, N. A. Kotov, S. Magonov, B. Ozturk, *Nat. Mater.* **2**, 413 (2003).
7. A. Sellinger *et al.*, *Nature* **394**, 256 (1998).
8. W. J. Clegg, *Science* **286**, 1097 (1999).
9. M. G. Worster, J. S. Wettlaufer, *J. Phys. Chem. B* **101**, 6132 (1997).
10. S. W. Sofie, F. Dogan, *J. Am. Ceram. Soc.* **84**, 1459 (2001).
11. H. Ishiguro, B. Rubinsky, *Cryobiology* **31**, 483 (1994).
12. J. O. M. Karlsson, *Science* **296**, 655 (2002).
13. G. Gay, M. A. Azouni, *Cryst. Growth Des.* **2**, 135 (2002).
14. A. P. Jackson, J. F. V. Vincent, R. M. Turner, *Proc. R. Soc. Lond. Ser. B* **234**, 415 (1988).
15. J. Aizenberg *et al.*, *Science* **309**, 275 (2005).
16. R. Z. Wang, Z. Suo, A. G. Evans, N. Yao, I. A. Aksay, *J. Mater. Res.* **16**, 2485 (2001).
17. F. Song, A. K. Soh, Y. L. Bai, *Biomaterials* **24**, 3623 (2003).
18. E. Saiz, R. M. Cannon, A. P. Tomsia, *Acta Mater.* **48**, 4449 (2000).
19. L. L. Hench, J. M. Polak, *Science* **295**, 1014 (2002).
20. T. Dutta Roy, J. L. Simon, J. L. Ricci, E. D. Rekow, V. P. Thompson, J. R. Parsons, *J. Biomed. Mater. Res.* **66A**, 283 (2003).
21. Y. H. An, in *Mechanical Testing of Bone and the Bone-Implant Interface* (CRC Press, Boca Raton, FL, 2000), pp. 41–63.
22. A. Almirall *et al.*, *Biomaterials* **25**, 3671 (2004).
23. R. P. del Real, J. G. C. Wolke, M. Vallet-Regi, J. A. Jansen, *Biomaterials* **23**, 3673 (2002).
24. Y. Ota, T. Kasuga, Y. Abe, *J. Am. Ceram. Soc.* **80**, 225 (1997).
25. A. Bignon, thesis, National Institute of Applied Science, Lyon, France (2002).
26. H. R. Ramay, M. Q. Zhang, *Biomaterials* **24**, 3293 (2003).
27. M. Sous *et al.*, *Biomaterials* **19**, 2147 (1998).
28. D. M. Liu, *Ceram. Int.* **23**, 135 (1997).
29. M. Milosevski, J. Bossert, D. Milosevski, N. Gruevska, *Ceram. Int.* **25**, 693 (1999).
30. M. Kawata *et al.*, *J. Mater. Sci. Mater. Med.* **15**, 817 (2004).

31. This work was supported by the NIH National Institute of Dental and Craniofacial Research under grant 5R01 DE015633 ("Complex nanocomposites for bone regeneration") and by the Director, Office of Science, Office of Basic Energy Sciences, Division of Materials Sciences and Engineering of the U.S. Department of Energy under contract DE-AC03-76SF00098 (Metal/Ceramic Composites). The authors wish to thank R. O. Ritchie for useful discussions and J. Wu for help with the synthesis of the aluminum-infiltrated composites.

Supporting Online Material

www.sciencemag.org/cgi/content/full/311/5760/515/DC1
Materials and Methods
Figs. S1 and S2

4 October 2005; accepted 6 December 2005
10.1126/science.1120937

The Cellular Basis of a Corollary Discharge

James F. A. Poulet[1,2]* and Berthold Hedwig[2]

How do animals discriminate self-generated from external stimuli during behavior and prevent desensitization of their sensory pathways? A fundamental concept in neuroscience states that neural signals, termed corollary discharges or efference copies, are forwarded from motor to sensory areas. Neurons mediating these signals have proved difficult to identify. We show that a single, multisegmental interneuron is responsible for the pre- and postsynaptic inhibition of auditory neurons in singing crickets (*Gryllus bimaculatus*). Therefore, this neuron represents a corollary discharge interneuron that provides a neuronal basis for the central control of sensory responses.

An animal's behavior generates a constant flow of sensory information that can update or fine-tune ongoing motor activity (*1*) but can also desensitize the animal's own sensory pathways and/or be confused with external stimuli. One solution to these problems is to forward a signal, or corollary discharge, from motor to sensory regions during behavior to counter the expected, self-generated sensory feedback (*2*, *3*). A role for corollary discharges

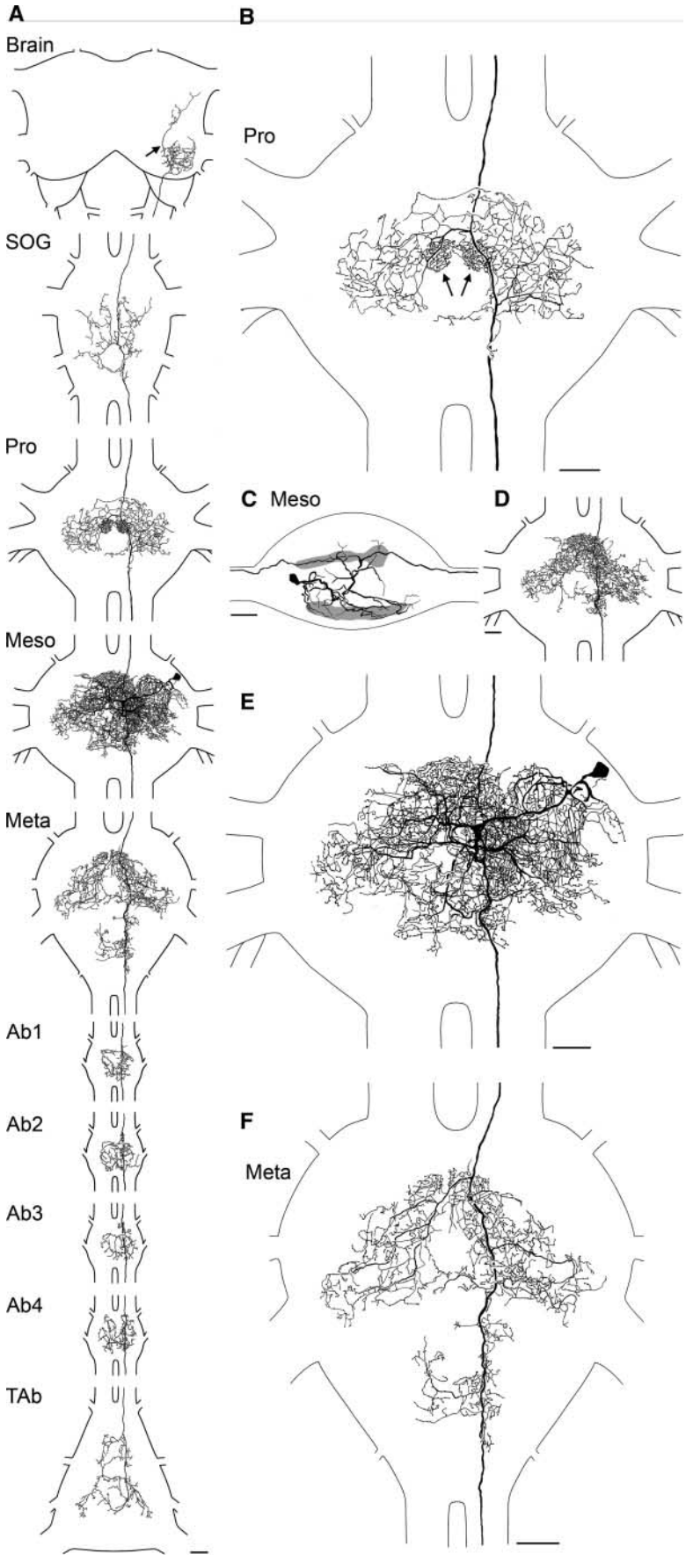

Fig. 1. Morphology of CDI. (**A**) A whole-mount staining of CDI in the CNS of an adult male *G. bimaculatus* in ventral view. The soma and dendrites are located in the mesothoracic ganglion, and two axons project throughout the whole CNS with extensive varicose arborizations that are bilateral in every ganglion except the brain. Arrow in brain indicates anterior branch of CDI stained in two of six stainings of its axon in the brain. (**B**) Axonal arborizations in the prothoracic ganglion; arrows indicate overlap with the auditory neuropils. (**C**) Lateral view of CDI in mesothoracic ganglion. The soma is positioned medially near the dorsolateral edge of the ganglion. From the soma the primary neurite extends in a loop toward the middle of the ganglion and gives off a widespread bilateral array of smooth branches typical of insect dendrites. Two axons originate centrally in the ganglion and extend both anteriorly and posteriorly. (**D**) Ventral axonal arborizations in the mesothoracic ganglion. (**E**) Dendritic (dorsal) and axonal (ventral) arborizations of CDI in the mesothoracic ganglion. (**F**) Axonal arborizations of CDI in the metathoracic ganglion have a similar morphology to those in the mesothoracic ganglion. Abbreviations: SOG, suboesophageal ganglion; Pro, prothoracic ganglion; Meso, mesothoracic ganglion; Meta, metathoracic ganglion; Ab1 to Ab4, abdominal ganglia 1 to 4; TAb, terminal abdominal ganglion. Scale bars, 100 μm.

in modifying sensory processing during behavior has been identified in many sensory systems (*4*–*11*). Despite their ubiquity and importance, however, very little is known about the neurons mediating corollary discharges.

An ideal model system to analyze a corollary discharge is the singing male cricket (*6*, *12*). Cricket song is composed of a series of 100 dB SPL chirps, repeated every 300 to 500 ms, each containing three to five sound pulses or syllables. Sound is generated during the closing movements of the wing. The crickets' ears are located on their forelegs and remain fully sensitive during singing (*13*). Therefore the cricket's central nervous system (CNS) has to deal with a massive influx of auditory, proprioceptive, and mechanoreceptive information during sound production. Crickets maintain auditory sensitivity during singing by inhibiting their central auditory pathway with a corollary discharge in phase with sound production (*14*). In this study, we identify the neuron that mediates this corollary discharge.

The corollary discharge interneuron (CDI) was physiologically identified by simultaneous intracellular recordings of auditory neurons in the prothoracic ganglion, where primary auditory signals are processed, and systematic probing of interneurons in the mesothoracic ganglion, which houses part of the singing pattern generating network. Consecutive stainings (n = 12 crickets) revealed its extensive branching pattern throughout the CNS (Fig. 1) (*15*).

[1]Laboratory of Sensory Processing, Brain Mind Institute, École Polytechnique Fédérale de Lausanne, CH-1015 Lausanne, Switzerland. [2]Department of Zoology, University of Cambridge, Cambridge CB2 3EJ, UK.

*To whom correspondence should be addressed. E-mail: james.poulet@epfl.ch

The morphology of CDI highlights three major structural properties that are crucial for its function. First, its cell body and extensive dendritic arborization is in the mesothoracic ganglion; therefore, it can receive synaptic input from the singing central pattern generator (CPG). Second, the neuron has profuse axonal arborizations that overlap with the auditory neuropil in the prothoracic ganglion, a prerequisite to forming direct output synapses with auditory neurons. Third, its axon targets widespread areas of the CNS and could affect other sensory pathways activated during singing.

Recordings from CDI were made from its dendritic branches during pharmacologically elicited fictive singing, with all thoracic sensory and motor nerves cut except for the auditory nerves (*3*, *15*). CDI generates bursts of spikes in synchrony with the wing motoneuron activity indicating the chirps (Fig. 2A). CDI spikes reach frequencies of 131 ± 16 Hz during the first syllable of the chirp and a maximum of 178 ± 9 Hz during the following syllables (mean ± SEM; n = 18). Quantitative analysis reveals that each burst of spikes occurred during wing-closing motor activity (stippled lines in Fig. 2B). This corresponds to the phase of wing movements when sound is produced and also with the timing of inhibitory inputs in auditory neurons during singing (*14*). To test whether CDI is part of the singing CPG, we used 100-ms depolarizing current pulses to elicit spikes and measured any effect on the singing motor pattern (Fig. 2C). Elicited bursts of spikes in CDI never had an effect on the timing of the ongoing singing motor pattern (n = 10) (Fig. 2D). Singing also continued normally when CDI was prevented from spiking by injection of hyperpolarizing current (n = 10). We therefore conclude that CDI is not part of the singing CPG but instead is driven by it.

Because CDI receives excitatory input during wing-closing movements, we tested whether it might also be activated during flying. When the crickets generated the flight motor pattern (n = 7), CDI was always inhibited by a barrage of inhibitory postsynaptic potentials (IPSPs) (Fig. 2, E and F), as were some of the neurons thought to be part of the cricket singing CPG (*16*). CDI did not respond to 85 dB SPL acoustic stimulation at 4.8 kHz, the carrier frequency of cricket song (n = 10) (Fig. 2G).

CDI's anatomy and physiology strongly suggested that it could mediate pre- and postsynaptic inhibition of the auditory pathway during singing (*3*). Paired intracellular recordings from CDI's dendrite and auditory neurons revealed the synaptic connectivity. About 60 auditory afferent neurons extend from the cricket's ears in the forelegs into prothoracic ganglion, where they terminate in a median-ventral auditory neuropil (*17*). Here they forward excitatory information onto a small number of auditory interneurons such as the local omega neuron 1 (ON1) (*18*). Paired recordings from CDI and auditory afferent axonal arborizations demonstrated that spikes in CDI occurred in synchrony with primary afferent depolarizations (PADs) during wing-closing motor activity (Fig. 3A). PADs cause a reduction in spike height in cricket auditory afferents (*14*) and mediate presynaptic inhibition in a number of sensory systems (*19*–*21*). When depolarizing current was injected into CDI, each spike in CDI reliably elicited a PAD of 2.0 ± 0.2 mV in the auditory afferent after a constant latency of 3.8 ± 0.1 ms (n = 7) (Fig. 3, B and C). Paired recordings of CDI and ON1 (Fig. 3D) revealed that ON1 received IPSPs when CDI spiked during a chirp. Injection of current into CDI revealed that each CDI spike elicited an IPSP of 1.6 ± 0.2 mV in ON1 after a delay of 3.5 ± 0.2 ms (n = 8) (Fig. 3, E and F). CDI has bilateral arborizations in the pro-

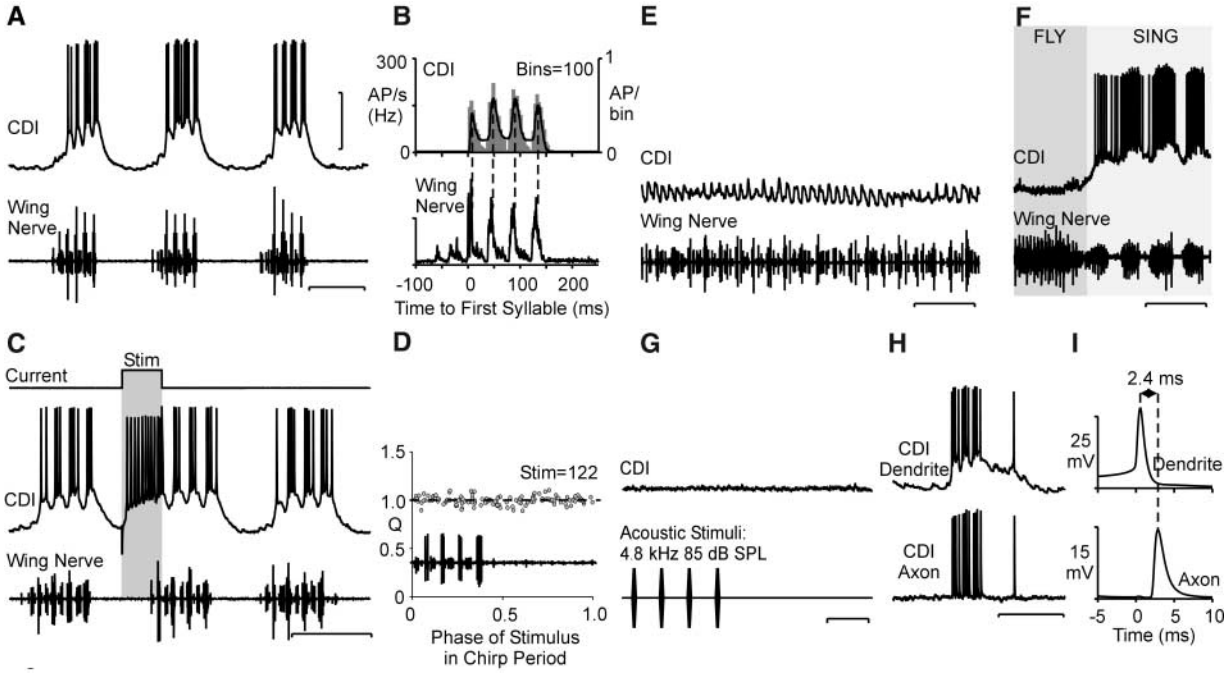

Fig. 2. Recordings of CDI and wing motor nerve during fictive singing and flight. (**A**) Spikes in CDI as recorded in the dendrite during fictive chirps. (**B**) The PSTH and superimposed instantaneous spike rate (n = 59 chirps, 759 spikes) with the averaged wing motor nerve activity demonstrate that CDI fires bursts of spikes during the wing-closing motor activity of each chirp, as indicated by the stippled lines. (**C**) Injection of depolarizing current into CDI elicited bursts of spikes but did not change the ongoing singing pattern. (**D**) Phase response curve. Q = (duration of ongoing chirp period N)/(duration of chirp period N + 1) at the phase of stimulation of CDI with a current pulse of 100 ms. Analysis shows no modulation in the duration of chirps by CDI stimulation. (**E**) CDI is rhythmically inhibited during fictive flight. (**F**) Transition from fictive flight to fictive singing demonstrates the change in activity. (**G**) CDI does not respond to acoustic stimulation with 4.8 kHz, 85 dB SPL pulses 21 ms in duration. (**H**) Paired recording from the dendrite in the mesothoracic ganglion and axon in the prothoracic auditory neuropil of the same CDI. (**I**) Average of paired recording from the same CDI shows, in this example, a delay of 2.4 ms from spike recorded in the dendrite to spike recorded in the axon in the prothoracic ganglion (n = 181 spikes). CDI, intracellular CDI recording; Wing Nerve, activity of mesothoracic nerve 3A. Vertical scale bars, 20 mV [(A), (C), (F), (G), and dendrite in (H)], 10 mV [(E) and axon in (H)]; horizontal scale bars, 250 ms [(A), (G), (H)], 200 ms [(C) and (E)], 1 s (F).

thoracic ganglion, and spikes in CDI elicited IPSPs and PADs in both the left- and right-side ON1s and afferents. Paired recordings of CDI in its dendrite and prothoracic axon showed that CDI spikes take 2.8 ms to reach the auditory neuropil (n = 4) (Fig. 2, H and I), which leaves less than 1 ms from the spike in the prothoracic ganglion to the release of IPSPs or PADs. We never recorded a failure of an IPSP or PAD in response to a CDI spike. Therefore, both the anatomical evidence of axonal arborizations of CDI in the auditory neuropil and the physiological evidence suggest that the connection from CDI to auditory afferents and to ON1 is monosynaptic.

What effect does CDI have on auditory processing? Paired recordings were obtained from CDI and ON1 during continuous presentation of computer-generated sound pulses at the carrier frequency of cricket song (Fig. 4). In resting crickets, when CDI was not spiking, the sound pulses elicited a train of spikes in ON1. When CDI was depolarized to make it spike, the auditory response in ON1 was inhibited (Fig. 4, A and B). During silent, fictive singing, ON1's response to the external sound stimuli was suppressed during the chirps, even when one CDI was prevented from spiking by injecting hyperpolarizing current (n = 8) (*22*). Because CDI exists as a bilateral pair of neurons, both with bilateral outputs, the persisting inhibition was most likely due to spikes in CDI's contralateral partner cell. However, we could not rule out the possibility of parallel inhibitory neurons. To examine whether the CDIs are the only neurons mediating the inhibition of the auditory pathway, we made a paired recording of CDI and ON1 during singing and then cut the contralateral prothoracic-to-mesothoracic connective, which contained the axon of the partner CDI (n = 2). When the animal's singing recovered, ON1 was inhibited by CDI during fictive singing and failed to respond to the ongoing auditory stimuli (Fig. 4, C and D). When CDI was hyperpolarized and prevented from spiking, ON1 responded to the sound pulses both in the chirp interval and in the chirp (Fig. 4, E and F). This confirmed that CDI is both sufficient and necessary to mediate the corollary discharge inhibition during singing, and there is no evidence for any parallel inhibitory pathways.

Over the past 50 years, investigation into the cellular basis of corollary discharges and efference copies has been hampered by a lack of data on identified neurons mediating these signals. There are now only a small number of neurons thought to mediate corollary discharges (*5*, *23*–*26*). The synaptic connectivity has been explored with intracellular recordings in only two populations of neurons (*25*, *26*). CDI is a rare example of a functionally and anatomically identified neuron that extends throughout the entire insect nervous system. Simultaneously, CDI mediates the presynaptic inhibition of auditory afferents with PADs and the postsynaptic inhibition of an identified auditory interneuron with IPSPs. This twofold inhibition reduces the auditory response to self-generated sounds and protects the cricket's auditory pathway from desensitization during sound production, allowing it to remain sensitive to environmental sounds (*6*, *12*, *14*). Thus, even in the small nervous system of the cricket, self-generated sensory signals are processed in a similar way to more complex vertebrate nervous systems (*27*, *28*). During flight, CDI is inhibited and prevented from firing; hence, flying crickets' hearing will not be impeded by CDI and they can listen for signaling conspecifics or echolocating calls from predating bats (*29*). The singing cricket also generates substantial nonauditory sensory feedback [e.g., (*30*)]. The complex and widespread branches of CDI indicate that it may also inhibit other sensory pathways. CDI therefore provides an opportunity to understand not only the role of timing in corollary discharge signals but also the computation by which motor and sensory signals are integrated.

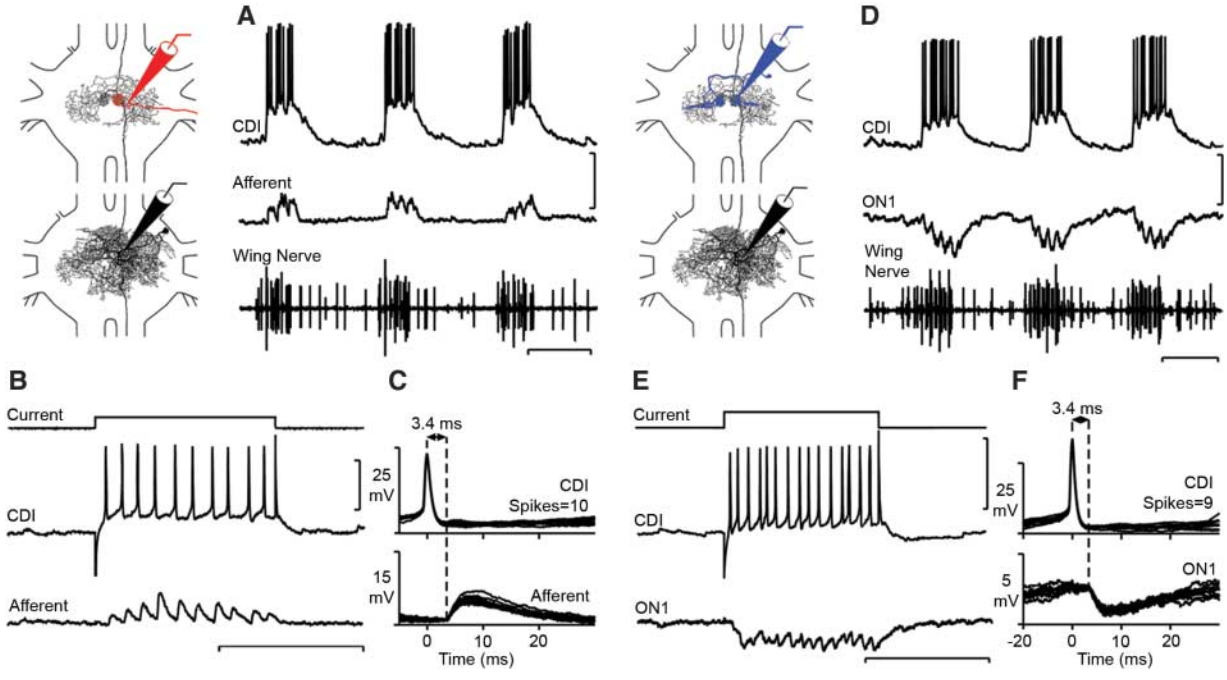

Fig. 3. Inhibitory inputs in auditory neurons are elicited by CDI spikes. (**A**) Paired recording of CDI and an auditory afferent during singing. Spikes in CDI coincide with PADs in the afferent. (**B**) Stimulation of CDI with intracellular depolarizing current injection. Each CDI spike elicits a PAD in the afferent. (**C**) Superposition of CDI and afferent recording triggered by spikes in CDI. In this example, PADs were elicited after a constant delay of 3.4 ms from CDI spike. (**D**) Paired recording of CDI and ON1 during singing. Spikes in CDI coincide with IPSPs in ON1. (**E**) Every spike elicited by depolarizing current injection in CDI elicits an IPSP in ON1. (**F**) Superimposed traces of CDI and ON1 show a constant latency (in this example 3.4 ms) from CDI spike to the IPSP. Afferent: intracellular auditory afferent recording; ON1, intracellular ON1 recording. Vertical scale bars, CDI: 15 mV (A), 30 mV (B), 20 mV (D), 25 mV (E); ON1: 15 mV (D), 5 mV (E); afferent: 20 mV (A), 10 mV (B); current: 5 nA; horizontal scale bars, 250 ms [(A) and (D)], 200 ms [(B) and (E)].

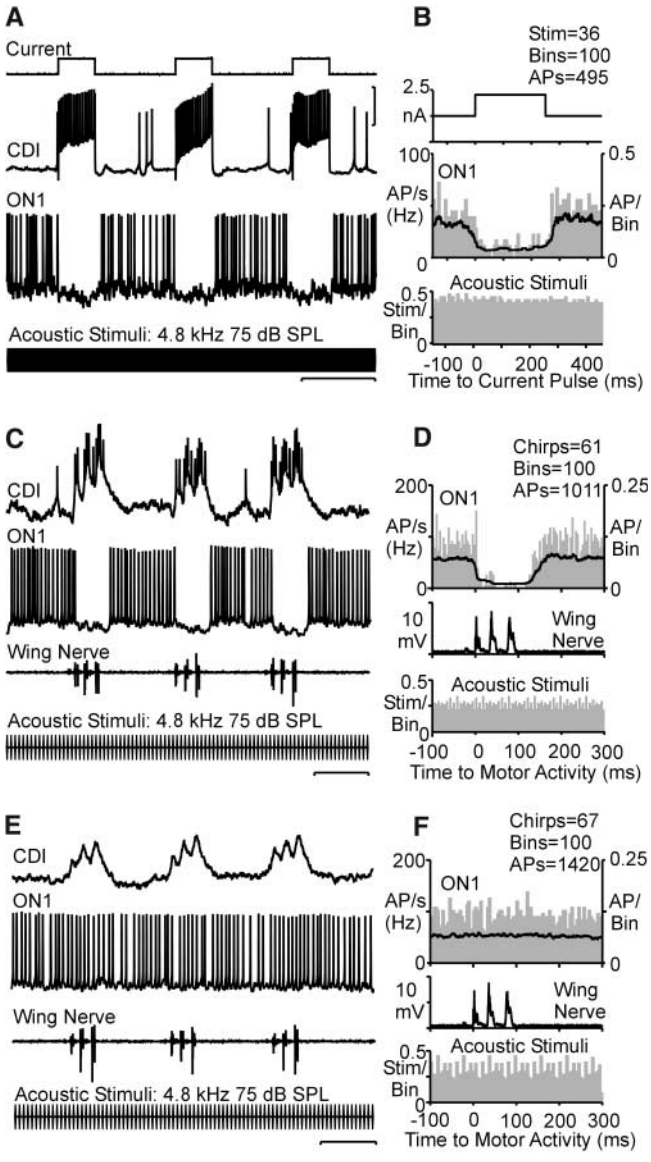

Fig. 4. The effect of CDI on sound processing. (**A**) ON1's response to a continuous sequence of 4.8 kHz, 75 dB SPL sound pulses, 8 ms in duration with intervals of 7 ms, is completely inhibited during periodic current injection in CDI. (**B**) PSTH and superimposed instantaneous spike frequency of ON1 averaged over 36 trials demonstrate that ON1 activity is reduced during CDI stimulation. (**C**) In an animal with the contralateral prothoracic-to-mesothoracic connective cut, ON1 responds with a train of spikes during the chirp intervals, but it fails to respond during the chirp if CDI is spiking. (**D**) The PSTH and instantaneous spike frequency of ON1 highlights the reduction in ON1 response during the chirp. (**E**) When CDI is prevented from spiking by hyperpolarizing current injection, ON1 responds to sound during the chirp and the chirp interval. (**F**) When CDI spikes were suppressed by inhibitory current injection, the PSTH and instantaneous spike frequency show no reduction in the activity of ON1 during chirps. Vertical scale bar, current: 2.5 nA (A); CDI: 20 mV [(A) and (E)], 10 mV (C); ON1: 20 mV [(A), (C), and (E)]; horizontal scale bars, 500 ms (A), 200 ms [(C) and (E)].

References and Notes

1. K. G. Pearson, *Annu. Rev. Neurosci.* **16**, 265 (1993).
2. R. W. Sperry, *J. Comp. Physiol. Psychol.* **43**, 482 (1950).
3. E. von Holst, H. Mittelstaedt, *Naturwissenschaften* **37**, 464 (1950).
4. M. Zaretsky, C. H. F. Rowell, *Nature* **280**, 583 (1979).
5. M. A. Sommer, R. H. Wurtz, *Science* **296**, 1480 (2002).
6. J. F. A. Poulet, B. Hedwig, *Nature* **418**, 872 (2002).
7. K. T. Sillar, P. Skorupski, *J. Neurophysiol.* **55**, 678 (1986).
8. K. T. Sillar, A. Roberts, *Nature* **331**, 262 (1988).
9. S. J. Blakemore, D. Wolpert, C. D. Frith, *Nat. Neurosci.* **1**, 635 (1998).
10. C. C. Bell, *Science* **214**, 450 (1981).
11. J. E. Roy, K. E. Cullen, *J. Neurosci.* **24**, 2102 (2004).
12. J. F. A. Poulet, B. Hedwig, *J. Neurosci.* **23**, 4717 (2003).
13. J. F. A. Poulet, B. Hedwig, *J. Exp. Biol.* **204**, 1281 (2001).
14. J. F. A. Poulet, B. Hedwig, *J. Neurophysiol.* **89**, 1528 (2003).
15. See supporting material on *Science* Online.
16. R. M. Hennig, *J. Comp. Physiol. A* **167**, 629 (1990).
17. K. Michel, *Z. Morph. Tiere* **77**, 285 (1974).
18. K. Schildberger, D. W. Wohlers, F. Huber, in *Cricket Behavior and Neurobiology*, F. Huber, T. E. Moore, T. E. Loher, Eds. (Cornell Univ. Press, Ithaca, NY, 1989), pp. 423–458.
19. M. D. Kirk, J. J. Wine, *Science* **225**, 854 (1984).
20. F. Clarac, D. Cattaert, *Exp. Brain Res.* **112**, 163 (1996).
21. P. Rudomin, R. F. Schmidt, *Exp. Brain Res.* **129**, 1 (1999).
22. J. F. A. Poulet, B. Hedwig, data not shown.
23. M. G. Weeg, B. R. Land, A. H. Bass, *J. Neurosci.* **25**, 5967 (2005).
24. C. C. Bell, K. Dunn, C. Hall, A. Caputi, *J. Comp. Physiol. A* **177**, 449 (1995).
25. W. C. Li, S. R. Soffe, A. Roberts, *J. Neurosci.* **22**, 10924 (2002).
26. S. C. Rosen, M. W. Miller, E. C. Cropper, I. Kupfermann, *J. Neurophysiol.* **83**, 1621 (2000).
27. K. E. Cullen, *E. Curr. Op. Neurobiol.* **14**, 698 (2004).
28. C. C. Bell, K. Grant, *J. Neurosci.* **9**, 1029 (1989).
29. T. G. Nolen, R. R. Hoy, *Science* **226**, 992 (1983).
30. M. Dambach, H.-G. Rausche, G. Wendler, *Naturwissenschaften* **70**, 417 (1983).

31. We thank S. Atkinson, M. Burrows, C. Petersen, and S. Rogers for comments on the manuscript. Supported by the UK Biotechnology and Biological Sciences Research Council, the Royal Society, and the Human Frontier Science Program.

Supporting Online Material

www.sciencemag.org/cgi/content/full/311/5760/518/DC1
Materials and Methods
References

3 October 2005; accepted 20 December 2005
10.1126/science.1120847

Scaling of Connectivity in Marine Populations

R. K. Cowen,[1]* C. B. Paris,[1] A. Srinivasan[2]

Defining the scale of connectivity, or exchange, among marine populations and determining the factors driving this exchange are pivotal to our understanding of the population dynamics, genetic structure, and biogeography of many coastal species. Using a high-resolution biophysical model for the Caribbean region, we report that typical larval dispersal distances of ecologically relevant magnitudes are on the scale of only 10 to 100 kilometers for a variety of reef fish species. We also show the importance of the early onset of active larval movement mediating the dispersal potential. In addition to self-recruitment, larval import from outside the local area is required to sustain most populations, although these population subsidies are very limited in particular systems. The results reveal distinct regions of population isolation based on larval dispersal that also correspond to genetic and morphological clines observed across a range of marine organisms.

Identifying the scale of marine larval dispersal remains one of the fundamental challenges to marine ecology and oceanography. Most coastal marine species have limited adult movement, so the relatively short, pelagic larval phase represents the primary opportunity for dispersal. Although larvae have the potential for long-distance dispersal (*1*, *2*), evidence is mounting that larval dispersal may be limited (*3*–*11*). These studies challenge assumptions about the dominant distance mode of dispersal for marine populations (whether larvae typically travel a long or short distance) (*12*, *13*). The rates, scale, and spatial structure of successful exchange, or connectivity, among local populations of marine organisms drive population replenishment and, therefore, have profound implications for population dynamics and genetics of marine organisms; spatially oriented resource management (e.g., marine protected areas); and the

[1]Marine Biology and Fisheries, [2]Meteorology and Physical Oceanography, Rosenstiel School of Marine and Atmospheric Science, University of Miami, 4600 Rickenbacker Causeway, Miami, FL 33149, USA.

*To whom correspondence should be addressed. E-mail: rcowen@rsmas.miami.edu